Frequency-selective near-field radiative heat transfer between photonic-crystal slabs: A computational approach for arbitrary geometries and materials

Alejandro W. Rodriguez,[1,2] Ognjen Ilic,[3] Peter Bermel,[3] Ivan Celanovic,[3]
John D. Joannopoulos,[3] Marin Soljačić,[3] and Steven G. Johnson[2]

[1]*School of Engineering and Applied Sciences, Harvard University, Cambridge, MA 02138*
[2]*Department of Mathematics, Massachusetts Institute of Technology, Cambridge, MA 02139*
[3]*Department of Physics, Massachusetts Institute of Technology, Cambridge, MA 02139*

We demonstrate the possibility of achieving enhanced frequency-selective near-field radiative heat transfer between patterned (photonic crystal) slabs at designable frequencies and separations, exploiting a general numerical approach for computing heat transfer in arbitrary geometries and materials based on the finite-difference time-domain method. Our simulations reveal a tradeoff between selectivity and near-field enhancement as the slab–slab separation decreases, with the patterned heat transfer eventually reducing to the unpatterned result multiplied by a fill factor (described by a standard proximity approximation). We also find that heat transfer can be further enhanced at selective frequencies when the slabs are brought into a glide-symmetric configuration, a consequence of the degeneracies associated with the non-symmorphic symmetry group.

PACS numbers:

Radiative transfer of energy from a hot to a cold body is well known to be enhanced (even exceeding the blackbody limit) when the bodies are brought close enough for evanescent fields to contribute flux [1–9]. In this paper, we demonstrate that near-field radiative transfer can be greatly modified by using periodically patterned photonic-crystal (PhC) surfaces, with frequency-selective enhancement that can be controlled by choosing the geometry (rather than relying on material or plasmon resonances available only at long wavelengths [10–12]). Until now, investigations of near-field transfer in microstructured geometries have been hampered by the lack of computational modelling techniques, and we employ a new rigorous approach based on directly simulating Maxwell's equations in time with random thermal sources, an extension of the Langevin approach we previously used to model the emissivity of a single body [13]. Previously, aside from semi-analytical results for planar structures [11, 14, 15], formulations have been developed that in principle handle arbitrary geometries but which thus far have only been evaluated using Fourier methods specialized only for pairs of spheres and/or plates [16–21]. Multilayer planar structures are tractable [22], but (Fabry–Perot) resonant modes created in such structures are not evanescent in the air gap, unlike leaky modes in transverse-patterned structures (each of which has *both* evanescent and propagating fields in the gap), so multilayer films do not lend themselves to frequency-selective near-field enhancement. In the far field, it is known that more complicated structures such as PhCs can be designed to resonantly enhance radiative transfer at desired frequencies [23–25], which is crucial for applications such as thermophotovoltaic cells in which only certain frequencies can be efficiently converted to power [9, 25–27]. One would like to obtain similar short-wavelength ($\lesssim 2\,\mu$m [25]) enhancement of near-field effects, whereas plasmon resonances are too long-wavelength for such applications. In a simple model system consisting of two PhC slabs, thin films with periodic grooves [Fig. 1(top)], we show that the resonant leaky modes created by the periodicity yield orders of magnitude enhancement in the flux at designable wavelengths even for moderate separations (100s of nm to microns for infrared wavelengths) compared to similar structures in the far field, starting with weakly absorbing thin slabs that transfer $< 1/1000$ of the flux between black bodies in the far field. Furthermore, we show that the selective enhancement can be almost doubled at selective peaks by using a glide-symmetric configuration [Fig. 3(bottom)], due to degeneracies resulting from the properties of the non-symmorphic symmetry group [28]. Ultimately, there is a tradeoff between enhancement and frequency selectivity—much larger enhancement is theoretically attained for nm separations [4, 5, 7–9] where geometric resonances have no effect, at the cost of frequency selectivity and much more difficult fabrication—and this letter offers a first glimpse of the practical design space that is available to optimize these considerations.

Given two arbitrary bodies, at temperatures T_1 and T_2, their radiative heat transfer $H(\omega, T_1, T_2)$ is:

$$H(\omega; T_1, T_2) = \Phi(\omega)\left[\Theta(\omega, T_1) - \Theta(\omega, T_2)\right], \qquad (1)$$

where Φ is the flux into a single object due to random (white noise) current sources present in the other object, and Θ is the Planck distribution [9]. (Physically, for linear electromagnetism it is equivalent to use Planck-distributed thermal fluctuations or to use white-noise sources multiplied afterward by Θ.) Computationally, this formulation can be expressed directly in terms of a Langevin model [13], in which white-noise sources are introduced into the evolution of Maxwell's equations in

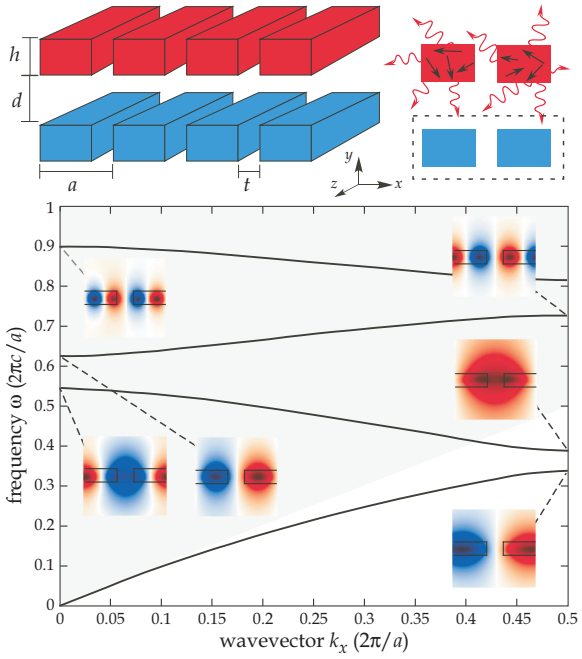

FIG. 1: Top: Schematic geometry of two PhC slabs of thickness $h = 0.2a$, separated by a distance d, with periodic air grooves of period a and width $t = 0.2a$. Bottom: Modal frequencies $\omega(k_x)$ of the TE ($\mathbf{H} \cdot \hat{\mathbf{z}} = 0$), $k_z = 0$ modes of an isolated slab; note the presence of both leaky (gray region) and guided modes. *Insets*: mode profiles at $k_x = \{0, \pi/a\}$.

a finite-difference time-domain (FDTD) method. (More sophisticated approaches for solving this problem exist, e.g. non-stochastic methods in the frequency domain, but the sacrifice in efficiency of our FDTD approach is compensated by its generality and simplicity.) Although we previously only applied this method to equilibrium situations [13], the extension to nonequilibrium situations is straightforward because the statistical independence of random currents in different objects allows one to calculate the flux due to thermal sources for one object at a time. Reciprocity allows one to calculate the flux Φ from one body to the other and infer the flux in the other direction, a fact that is implicit in Eq. (1).

We investigate the proof-of-concept structure shown in Fig. 1(top), involving two PhC dielectric slabs (thin films) of thickness $h = 0.2a$, separated by a distance d in the x direction, with z-oriented air grooves of period a and width $t = 0.2a$ in the x direction. The permittivity of the slabs is taken to be of the Drude form $\varepsilon(\omega) = \varepsilon_\infty - \sigma/\omega(\omega + i\gamma)$, where $\varepsilon_\infty = 12.5$, $\sigma = 0.2533\ (2\pi c/a)^2$, and $\gamma = 1.5915\ (2\pi c/a)$, approximating a dispersionless dielectric with $\mathrm{Re}\,\varepsilon \approx 12.5$ and $\mathrm{Im}\,\varepsilon \approx 1$ at wavelengths comparable to a. The computation of Φ for this structure involves introducing uncorrelated white-noise sources into the damped polarization equation [13] at each position (pixel) of one of the bodies [red slab in Fig. 1(top)], and integrating the resulting flux spectrum over a surface surrounding the other slab [blue slab in Fig. 1(top)]. The resulting spectrum is ensemble averaged over many simulations (~ 60) to reduce the noise level in the spectrum. We employ a periodic unit cell in x with Bloch-periodic boundaries (phase difference $e^{ik_x a}$), truncate the cell in the y direction using standard PML boundary conditions, and integrate Φ over k_x. The translation-invariant z direction can similarly be handled by integrating 2d simulations over k_z. We first consider the purely 2d problem corresponding to $k_z = 0$ and comment on the full 3d problem further below. At the moderately large separations $\sim a$ studied here (assuming a in the microns), the TE modes ($\mathbf{H} \cdot \hat{\mathbf{z}} = 0$) of the structure exhibit stronger confinement than the TM modes [29], and end up dominating the heat transfer at all relevant ω, and therefore we only compute the TE contribution.

Figure 1 plots the (TE, $k_z = 0$) modal frequencies $\omega(k_x)$ of a *single* (isolated) slab. Modes that lie in the gray region (above the $\omega = ck_x$ light line) are leaky modes [29], which radiate into the air and therefore contribute to heat transfer between the slabs in the far field. Modes that lie below the light line are guided modes [29], which evanescently decay in air and thus transfer energy only in the near field.

Figure 2(top) plots the flux enhancement $\eta = \Phi_{t,d}/\Phi_{0,\infty}$ as a function of ω, where $\Phi_{t,d}$ is the flux spectrum between PhC slabs of groove width t and separated by distance d, here normalized by the flux spectrum $\Phi_{0,\infty}$ of the unpatterned slabs ($t = 0$) in the far field ($d \to \infty$) to clearly illustrate the effect of finite t and d. ($\Phi_{0,\infty}$ is computed by Kirchoff's law from the reflectivity in the far field [4], by transfer-matrix methods.) The $\Phi_{0,\infty}$ spectrum by itself is nearly flat, so the spectral features in Fig. 2 are not due to the normalization. Note that we are starting with very weakly absorbing slabs (thin films), i.e. $\Phi_{0,\infty}$ is more than 1000 times smaller than the corresponding $\Phi = 1$ of two black bodies.

Radiative heat transfer can be significantly changed by the periodicity of the slabs [24], as illustrated by the green curve in Fig. 2(top), which shows η for PhCs of groove width $t = 0.2a$ in the far field. $\Phi_{0.2a,\infty}$ exhibits wide-bandwidth peaks, orders of magnitude larger than $\Phi_{0,\infty}$. Not surprisingly, the bandwidths of these peaks match the bandwidths of the leaky-mode bands in Fig. 1(bottom), whose integrated contribution over all k_y leads to a smearing of the sharp spectral peaks that occur at the leaky-mode frequencies for each k_y. The sharp drop in η between the peaks is a consequence of the presence of pseudogaps between the leaky-mode bands.

As the separation decreases, a number of dramatic features are observed in Fig. 2(top), which shows η at three additional separations ($d = 0.2a$, $d = 0.5a$ and $d = a$). At $d = a$, one can observe a dramatic increase in η at low frequencies. This arises due to the evanescent coupling and contribution of guided modes to h. This near-

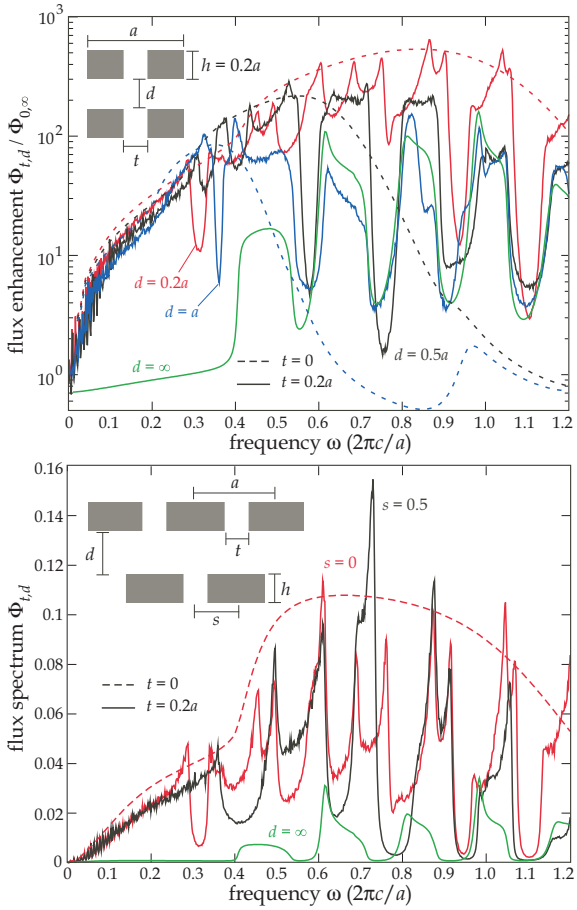

FIG. 2: Top: Flux enhancement $\eta = \Phi_{0.2a,d}/\Phi_{0,\infty}$ as a function of ω (units of $2\pi c/a$), where $\Phi_{t,d}$ is the flux spectrum between PhC slabs of groove width t and separation d, at various $d = 0.2a, 0.5a, a, \infty$. Solid (dashed) lines denote η for PhC (unpatterned) slabs. Bottom: Flux spectrum $\Phi_{0.2a,0.2a}$ [units of $\hbar c(2\pi/a)^2$] for a symmetric ($s = 0$, red line) or glide-symmetric ($s = 0.5a$, black line) slab–slab configuration.

field coupling increases further at smaller d, and additionally (especially in the $d = 0.2a$ curve) one can see a dip corresponding to the gap in the guided modes of Fig. 1(bottom), and sharp peaks at the edges of the gap (a consequence of van Hove singularities [29]). There is also an enhancement of Φ at small d at the leaky-mode peaks because, in a patterned slab, leaky-modes have an evanescent as well as a radiative component [29], and the former enhances the coupling at short distances. As for the guided modes, this evanescent coupling is further enhanced by the van Hove singularities of the zero-slope "slow-light" band edges. Also, the leaky modes split into bonding and antibonding pairs as d decreases, and a similar splitting is visible in the guided mode peaks at even smaller d, a phenomenon visible even more clearly in Fig. 2(bottom).

A striking phenomenon in the near-field interaction occurs when one patterned slab is shifted in the x direction by $0.5a$ with respect to the other slab, as shown in Fig. 2(bottom). In this case (plotted here as absolute Φ on a linear scale), the bonding-antibonding peaks of the symmetric configuration (solid red curve) *merge* at certain ω, and can even add to approximately double the heat transfer of the unpatterned slab. This arises due to the glide symmetry of the shifted structure, whose nonsymmorphic symmetry group supports degeneracies at the Brillouin zone edge ($k_x = \pi/a$) [28], causing the corresponding bonding-antibonding mode splittings to disappear. In contrast, the frequency splitting corresponding to the $k_x = 0$ band edges, e.g. at $\omega \approx 0.9$ ($2\pi c/a$), persists even for the glide-symmetric structure. Similarly, the gap in the guided modes of Fig. 1(bottom), near $\omega \approx 0.4$ ($2\pi c/a$), is greatly modified by the presence of the other slab in the mirror-symmetric case (red curve) but not in the glide-symmetric case (black curve).

Figure 2(top) also shows the enhancement for unpatterned ($t = 0$) slabs. These also exhibit a striking near-field enhancement for $d < a$, but in this case the enhancement is broad-band, because there are no standing-wave leaky-mode solutions in an unpatterned slab to induce frequency selectivity. In particular, at relatively large separations (e.g. $d = a$), the patterned slab exhibits more than 10 times the enhancement of the unpatterned slab, due to these resonant contributions. At $d = 0.5a$, the unpatterned slab is better for small ω and is worse for larger ω, where the latter is due to the fact that the evanescent interactions become shorter-range at high ω and vanish in the absence of resonant enhancement. At $d = 0.2a$, the unpatterned slab has larger enhancement over the whole bandwidth shown here, but lacks frequency selectivity. In general, as d decreases, the periodic structure of the PhC slabs ceases to matter, and the enhancement of the peaks relative to the overall near-field enhancement is lost. At even smaller d, not shown here, the interaction between the PhCs can be described by a proximity approximation in which adjacent surfaces are treated as parallel plates [5, 7–9] multiplied by a fill factor.

Figure 3 plots the total (integrated) heat transfer $H_{t,d}$ as a function of separation d for both patterned ($H_{t,d}$, squares) and unpatterned ($H_{0,d}$, thin lines) slabs of period $a = 2\mu$m, at various temperatures T_2, and $T_1 = 0$. At $T_2 = 500$ K, dominated by low-ω contributions, the unpatterned slabs yield larger H over almost every d (even as $d \to \infty$), which increases for small d due to near-field enhancement. Moreover, we find that $\xi = H_{t,d}/H_{0,d} \to 1 - t/a = 0.8$ as $d \to 0$, as expected from the proximity approximation. (For TE modes, H asymptotes to a finite value as $d \to 0$, whereas for TM modes, whose contributions are negligible at the separations we consider here, H eventually diverges [9].) At $T_2 = 1000$ K, larger ω begin to dominate, and the presence of PhC peaks [Fig. 2] causes a significant increase in H. In the (purely radiative) limit $d \to \infty$, the PhC slabs perform much better than the unpatterned slabs

($\xi \sim 3$), although the tradeoff between enhancement and selectivity is apparent as there exist a $d_c \approx 7$ μm below which $\xi < 1$ (eventually $\to 0.8$). As expected, d_c decreases as T_2 increases due to the increasing role of higher-frequency resonances. At $T_2 = 2000$ K, we find that $\xi \approx 5$ at larger d, increases at intermediate d and falls below 1 at $d_c \approx 2$ μm.

Figure 3 illustrates the advantages of using PhCs at large and intermediate d, where both selectivity and near-field effects coexist. However, in many applications, the figure of merit is not the overall H but the integrated H over a *finite frequency bandwidth*. In thermophotovoltaics, heat transferred from a hot body to a cold semiconductor is converted to electricity via electronic bandgap transitions, which means that photons of frequency smaller than the bandgap frequency ω_g (bandgap wavelength of a few microns) are lost in the conversion process [9]. The left inset of Fig. 3 shows a corresponding *ad hoc* figure of merit: the *windowed* heat transfer $H_w = \int d\omega\, H(\omega, T_1, T_2) n(\omega)$ between slabs of period $a = 1\mu$m, as a function of separation d, and at temperatures $T_1 = 300$ K and $T_2 = 1500$ K. The window function n is similar to the "quantum efficiency" function of a typical semiconductor of bandgap wavelength $2\pi c/\omega_g = 2.5$ μm [9]. The spectra $H(\omega)$ and $n(\omega)$ are plotted on the right inset of Fig. 3 at $d = 2$ μm. Noticeably, the presence of high-frequency peaks in the PhC makes its H_w over an order of magnitude larger than that of the unpatterned slab for $d \gtrsim 1\,\mu$m; the situation is even more favorable for the PhC because the low-frequency photons in the unpatterned case are wasted.

Our calculations of H were restricted to $k_z = 0$ for computational convenience. However, preliminary calculations of the k_z-integrated $H(\omega)$, for a single separation, reveal no qualitative changes in the spectrum, except for a slight broadening of the spectral peaks. As noted above, the geometry of Fig. 1 is in no way optimal and represents only a proof of concept: we believe that a 2d-periodic geometry will yield even better performance, an exciting direction for future numerical studies.

This work was supported by DARPA contract N66001-09-1-2070-DOD (AWR), by S3TEC, an Energy Frontier Research Center funded by the US DOE, Office of Science, and Office of Basic Energy Sciences, under award No. de-sc0001299, by the US ARO contract W911NF-07-D-0004, and through the Army Research Office through the Institute for Soldier Nanotechnologies under Contract No. W911NF-07-D0004 (OI, IC, PB).

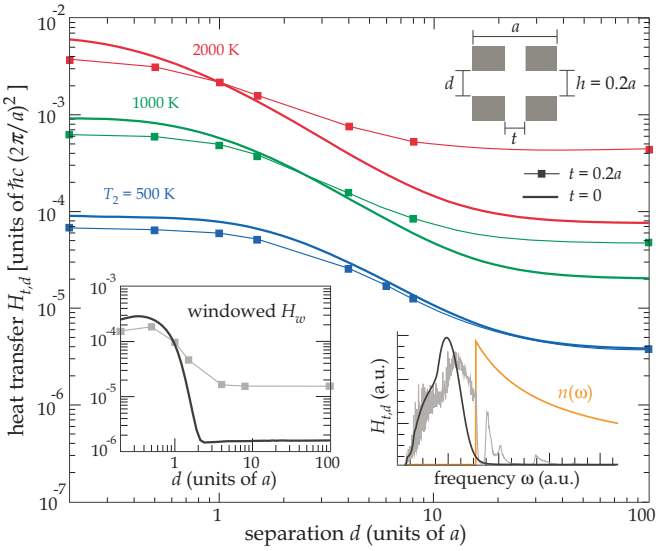

FIG. 3: Heat transfer $H_{t,d}$ [units of $\hbar c(2\pi/a)^2$] between unpatterned ($t = 0$, lines) or PhC ($t = 0.2a$, squares) slabs of period $a = 2\mu$m, as a function of d (units of a), plotted for $T_1 = 300$ K and various T_2. Left inset: h_w as a function of d (units of a) for slabs of period $a = 1\mu$m, and $T_2 = 1500$ K, where H_w is computed by windowing the spectrum $h(\omega)$ with a function that excludes contributions of wavelengths $> 2.5\,\mu$m. Right inset: $H_{t,d}$ (gray) and $H_{0,d}$ (black) at a typical separation $d = 2$ μm, and the window function $n(\omega)$ (orange line).

[1] D. Polder and M. Van Hove, Phys. Rev. B **4**, 3303 (1971).
[2] J. Loomis and H. Maris, Phys. Rev. B **50**, 18517 (1994).
[3] J. B. Pendry, J. Phys.: Condens. Matter **11**, 6621 (1999).
[4] M. Phillipe-Jean, K. Joulain, R. Carminati, and J.-J. Greffet, Micro. Therm. Eng. **6**, 209 (2002).
[5] K. Joulain, J.-P. Mulet, F. Marquier, R. Carminati, and J.-J. Greffet, Surf. Sci. Reports **57**, 59 (2005).
[6] V. P. Carey, G. Cheng, C. Grigoropoulos, M. Kaviany, and A. Majumdar, Nanoscale Micro. Thermophys. Eng. **12**, 1 (2006).
[7] A. I. Volokitin and B. N. J. Persson, Rev. Mod. Phys. **79**, 1291 (2007).
[8] Z. M. Zhang, *Nano/Microscale heat transfer* (McGraw-Hill, 2007).
[9] S. Basu, Z. M. Zhang, and C. J. Fu, Int. J. Energy Res. **33**, 1203 (2009).
[10] M. Francoeur, M. P. Menguc, and R. Vaillon, Appl. Phys. Lett. **93**, 043109 (2008).
[11] C. Fu and W. Tan, Journal of Quantitative Spectroscopy and Radiative Transfer **110**, 1027 (2009).
[12] S. Shen, A. Narayanaswamy, and G. Chen, Nano Letters **9**, 2909 (2009).
[13] C. Luo, A. Narayanaswamy, G. Ghen, and J. D. Joannopoulos, Phys. Rev. Lett. **93**, 213905 (2004).
[14] S. A. Biehs, Eur. Phys. J. B **58**, 423 (2007).
[15] W. T. Lau, J.-T. Shen, G. Veronis, and S. Fan, Phys. Rev. B **80**, 155135 (2009).
[16] A. Narayanaswamy and G. Chen, Phys. Rev. B **77**, 075125 (2008).
[17] G. Bimonte, Phys. Rev. A **80**, 042102 (2009).
[18] S.-B. Wen, J. Heat Transfer **132**, 072704 (2010).
[19] R. Messina and M. Antezza, arXiv **1012.5183**, 1 (2011).
[20] M. Krüger, T. Emig, and M. Kardar, Phys. Rev. Lett. **106**, 210404 (2011).
[21] C. Otey and S. Fan, arXiv **1103.2668**, 1 (2011).
[22] P. Ben-Abdallah, K. Joulain, and A. Pryamikov, Appl.

Phys. Lett. **96**, 143117 (2010).
[23] J.-J. Greffet, R. Carminati, K. Joulain, J.-P. Mulet, S. Mainguy, and Y. Chen, Nature **416**, 61 (2001).
[24] D. L. C. Chan, M. Soljačić, and J. D. Joannopoulos, Phys. Rev. E **74**, 016609 (2006).
[25] P. Bermel, et al., Optics Express **18**, A314 (2010).
[26] M. Whale and E. Cravalho, Energy Conversion, IEEE Transactions on **17**, 130 (2002).
[27] M. Laroche, R. Carminati, and J. J. Greffet, J. Appl. Phys. **100**, 063704 (2006).
[28] A. Mock, L. Lu, and J. O'Brien, Phys. Rev. B **81**, 155115 (2010).
[29] J. D. Joannopoulos, S. G. Johnson, J. N. Winn, and R. D. Meade, *Photonic Crystals: Molding the Flow of Light* (Princeton University Press, 2008), 2nd ed.